


Article

Inline NMR via a Dedicated V-Shaped Sensor

Eric Schmid ¹, Simon Rondeau ¹, Thomas Rudszuck ¹, Hermann Nirschl ¹ and Gisela Guthausen ^{1,2,*} 

¹ Institute of Mechanical Process Engineering and Mechanics, Karlsruhe Institute of Technology, 76131 Karlsruhe, Germany

² Engler-Bunte-Institut, Chair of Water Chemistry and Water Technology, Karlsruhe Institute of Technology, 76131 Karlsruhe, Germany

* Correspondence: gisela.guthausen@kit.edu

Abstract: Process monitoring and control require dedicated and reliable measures which reflect the status of the process under investigation. Although nuclear magnetic resonance is known to be a versatile analytical technique, it is only seldomly found in process monitoring. Single-sided nuclear magnetic resonance is one well known approach for being applied in process monitoring. The dedicated V-sensor is a recent approach that allows the inline investigation of materials in a pipe non-destructively and non-invasively. An open geometry of the radiofrequency unit is realized using a tailored coil, enabling the sensor to be applied for manifold mobile applications in in-line process monitoring. Stationary liquids were measured, and their properties were integrally quantified as the basis for successful process monitoring. The sensor, in its inline version, is presented along with its characteristics. An exemplary field of application is battery production in terms of anode slurries; thus, the first results on graphite slurries will demonstrate the added value of the sensor in process monitoring.

Keywords: low field NMR; inline process monitoring; relaxation; diffusion; NMR-sensor



Citation: Schmid, E.; Rondeau, S.; Rudszuck, T.; Nirschl, H.; Guthausen, G. Inline NMR via a Dedicated V-Shaped Sensor. *Sensors* **2023**, *23*, 2388. <https://doi.org/10.3390/s23052388>

Received: 23 January 2023

Revised: 13 February 2023

Accepted: 20 February 2023

Published: 21 February 2023



Copyright: © 2023 by the authors. Licensee MDPI, Basel, Switzerland. This article is an open access article distributed under the terms and conditions of the Creative Commons Attribution (CC BY) license (<https://creativecommons.org/licenses/by/4.0/>).

1. Introduction

Nuclear Magnetic Resonance (NMR) is well known in academia and industrial research in different experimental and instrumental designs. Two prominent examples are NMR spectroscopy, revealing information about chemical structures, and magnetic resonance tomography (MRT) in medical diagnostics. In industrial production with usually harsher environmental conditions, it is often used as at-line analytics in the form of low field (LF-)NMR, in the food and pharmaceutical industry, for example [1,2]. LF-NMR relies on permanent magnets and is therefore restricted by the magnetic remanence leading to magnetic fields/¹H Larmor frequencies, currently up to roughly 2.5 T/100 MHz [3]. Compared to high field NMR with ¹H Larmor frequencies commercially up to currently 1.2 GHz, the signals and the sensitivity are low as the population difference given by the Boltzmann law is significantly smaller. However, the instruments are much smaller and significantly more robust, which is essential for inline process monitoring.

Diverse parameters are known in NMR and also in LF-NMR. A multitude of contributions by a large number of researchers is known in the literature, and on development and applications of LF-NMR. A short and incomplete overview gives an impression about the diversity of the applied NMR methods: spectroscopy in chemical reaction monitoring and references therein [4–8]. Apart from spectroscopy, NMR relaxation reveals an insight into the materials studied as the measures rely on molecular dynamics. This kind of low-field NMR is prominently known in polymer research and applications, irrespective of whether it is measured integrally or spatially resolved, e.g., [9,10]. As the transverse relaxation rate, R_2 , is sensitive to low frequency fluctuations mainly within molecules, and as these fluctuations change upon chemical reaction and aging of macro-molecules, LF-NMR, relying on relaxation properties, was often applied in this context. Remarkable inventions were made

on the basis of permanent magnets regarding the applicability of NMR in the processes in biological context [11], as well as in process monitoring in harsher industrial environments and quality control, namely by the use of single-sided NMR [12–14]. In the present context, questions are addressed as to whether an open structure of an NMR sensor can be realized for process monitoring: Can material-characterizing properties be measured during flow, and is the sensitivity large enough to reliably control a process? What are the constraints concerning the pipe, its geometry and the flow rates? How can NMR sensitivity be optimized? An important prerequisite is that the sensor works completely non-invasively and non-destructively. Second, the pipe must not be opened for mounting the sensor. These prerequisites require dedicated hardware, which was addressed by simulation and technical realization. Finally, an example will be given which shows the usability of the sensor in a current application to batteries anode slurries.

2. Materials and Methods

The radio frequency (rf) probe was reconstructed for the V-shaped NMR-sensor [15] to allow for a mobile application in the context of monitoring the properties of a highly viscous, but flowing material. So far, the rf probe of the V-shaped sensor was realized in the conventional closed shape: the rf tank circuit was constructed by two trimmable capacitors and a solenoidal coil. Two regions of the magnet were used for NMR, one small cylindrical volume with moderate magnetic field gradient G of 0.35 T/m with a sample diameter of 12 mm, and the other larger volume in the outer part of the magnet with a sample diameter of 42 mm and a much larger magnetic field gradient up to 7 T/m, where the distribution of G within the sample volume is not negligible. Please note that the NMR signal is thus inherently sensitive to relaxation phenomena in the sample as well as to diffusion and convection, i.e., motional displacements. These facts were and are explored in single-sided NMR and other dedicated NMR sensors, e.g., [16]. The two places within the magnet were motivated by the application in lubricant quality control, requiring the compatibility with other established analytics concerning sample handling. The NMR-relevant properties of the two cylindrical regions in the V-shaped magnet needed to be considered in addition to the mentioned static magnetic field and its gradient, the rf field amplitude, its homogeneity, and the quality factor of the tank circuit which determines sensitivity and receiver dead time.

The off-line version, which was mainly used for lubricant quality control, is so far not well suited for inline process monitoring when postulating that the sensor should be removable and mobile without touching the process' material stream. Thus and primarily, the rf circuit needed a reconstruction and adaptation to these special requirements, which is the main topic of this paper (Sections 3 and 4), whereby the rf circuit provides the rf field for spin manipulation according to the NMR sequences.

The coil geometries (Sections 3 and 4) were simulated and characterized regarding their NMR properties: Larmor frequency $\nu_L(r)$ and the NMR-intensity $I(r)$ as function of the spatial coordinates within the sensitive area. The distance of the sample to be measured from the surface coil along y (Figure 1) must be mentioned. These parameters were measured using dedicated samples: A reference sample consisting of 20%w/w H_2O , 80%w/w D_2O and 0.1%w/w $CuSO_4$, and a graphite slurry for the production of anodes for lithium ion batteries (48.5%w/w graphite, 1%w/w carboxy methyl cellulose (CMC) and 0.5%w/w carbon black).

Methodical aspects are well known from single-sided NMR [17–23] and are applicable in the present form of the NMR V-sensor. Relaxation and diffusion/fluidic flow need to be considered in the magnetic field with its inherent static field gradients. These static magnetic field gradients provide the sensitivity towards molecular displacements, irrespective of whether they are due to statistical Brownian motion, of turbulent or coherent flow. Most often, multi echo sequences, also in the two-dimensional version of correlated experiments, are explored in which they allow the detection of mainly, but not exclusively, transverse magnetization decays [12,21,23–25].

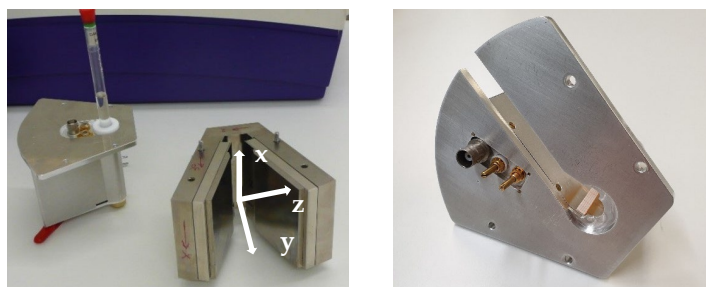


Figure 1. (Left): V-shaped NMR sensor (V-magnet with coordinate system and rf probe for off-line measurements) [15] and, on the (Right), the inline-capable rf probe. The probe is positioned in the magnets “V” so that the sample is aligned along x ((Left): typical 10 mm sample as used in low-field NMR). Since the inline probe ((Right) picture) has a slit, it can be easily mounted on tubes without opening the fluidic flow system. The rf connectors and the trim capacitors are also shown ((left): Reprinted/adapted with permission from Ref. [15]).

In a first approach, transverse magnetization decays are modelled by an exponential decay function, which is motivated by the basic Bloch equations of NMR, e.g., [26,27]. In the present case, neither the substances are simple liquids nor the technical equipment is ideal in the sense of NMR theory. Often the numerical approach of the inverse Laplace transform is applied in the literature, leading to an effective transverse relaxation time distribution [28–30]. It is well known that this approach is limited by the unavoidable experimental noise in the data, and further quantification is hampered by the fact that the distributions are complicated and by no means monomodal. A mathematical-analytical approach is also suitable. The Gamma distribution function was applied in previous works, e.g., on oils, and shows highly reproducible and physically interpretable results [31]. This approach considers that the magnetization relaxation is influenced by the distributions of material properties (disperse systems) and of technical parameters such as the magnetic field gradient, and the spatially varying flip angle of the rf pulses.

3. Results

3.1. Enabling Inline NMR-Measurements via the V-Shaped Sensor

A solenoidal coil geometry is most commonly used in LF-NMR devices because of the high signal-to-noise ratios compared to other coil geometries, and its suitability regarding the orientation of the magnetic fields. Further advantages concern the beneficial filling factor and the rf homogeneity. Despite this performance, a solenoidal coil is not well-suited for the inline-capable, mobile probe. These special requirements make a surface coil necessary to be mounted into the V-shaped magnet, which can then be flexibly positioned on an existing closed pipe. The loss of the signal-to-noise ratio using a surface coil leads to the motivation to optimize the coil geometry and its position.

Examples for the use of surface coils in low field NMR applications can be found in the literature. For example, McDonald et al. [32] developed the GARField magnet for sub-surface measurements in cement-based materials. Blümich et al. [12] used a surface coil for single-sided NMR with the MOUSE.

The approach in this work is to design a dedicated surface coil that fits the prerequisites of the addressed application. The coil is adapted to the geometry of a cylindrical pipe with a diameter of 10 mm. A bent figure-8 coil was developed and adapted to the intended application. It was compared to a spirally wound, bent surface coil.

3.1.1. Reconstruction of the RF Probe

The V-shaped magnet unit described in [12] was equipped with a closed probe for samples with a diameter up to 12 mm, measuring the samples volumetrically (Figure 1, left). The inline-capable probe now exhibits a characteristic slit (Figure 1, right), through which a tube can be placed near the surface coil without touching the process stream in any

form. The cover plate, made of aluminum, provides holes for the two match and tune trim capacitors and the rf connection to a commercial electronics unit (Bruker “the minispec” NF series). There are four holes to fix the probe to the magnet unit on a very defined position. The measuring volume is in the front area in analogy to the offline probe [12]. A conductive box is mounted directly under the cover plate, in which the match and tune trim capacitors and the wirings are placed. The purpose of the box is an efficient shielding of the environmental electromagnetic noise from the rf circuit and to decouple the magnet from the rf circuit. The magnet unit with the inserted probe has the following geometric dimensions: length: 11 cm; width: 13 cm; and height: 8 cm.

The rf circuit consists of two trim capacitors (Voltronics NMTM120CE) and the rf coil. The same capacitors were used for a comparison of the different coil geometries, and only the coil was exchanged. The different surface coils were mounted on a half-shell of the outer housing with rubber spacers for a defined and fixed positioning. The whole probe is designed for easy, subsequent adjustments and optimizations, including a change of the surface coil.

3.1.2. From Volume Coil to Surface Coil: Simulation of the RF Magnetic Field

Simulations of the RF fields, more specific to its magnetic part B_1 , of the two different coil geometries, were carried out in order to define an optimized coil geometry concerning the signal intensity and measuring depth. A spirally wound, bent surface coil was compared to a bent figure-8 coil. The software COMSOL Multiphysics, Version 6.0, was used for the simulations. The coil geometries were set as homogeneous multiturn coils to reduce the simulation’s computational costs. Thus, the current distribution within each winding of the inductor was neglected. The calculated absolute values of the amplitudes of magnetic flux density $|B_1(\mathbf{r})|$ are physically not exact, but its spatial profile and distribution are nevertheless relevant and reliable. The modelling of each and every turn of the coils could thus be avoided; nevertheless, the number of turns is considered by a specific parameter. To increase the reliability of the results related to the spatial distribution of the magnetic flux density, the actual value of the current through the coil was not implemented. Instead, the excitation current was set to an arbitrary value of 4 A.

The simulation of the spirally wound, bent surface coil (Figure 2) shows a condensation of the field lines along x above and below the opening of the coil. Two condensation areas of the field lines appear for the figure-8 coil (Figure 3) at both openings of the coil. The simulated y -profile (Figure 4) shows that $|B_1|$ is considerably larger for the figure-8 coil than for the spirally wound, bent coil, up to a distance from the coil’s surface of 9 mm.

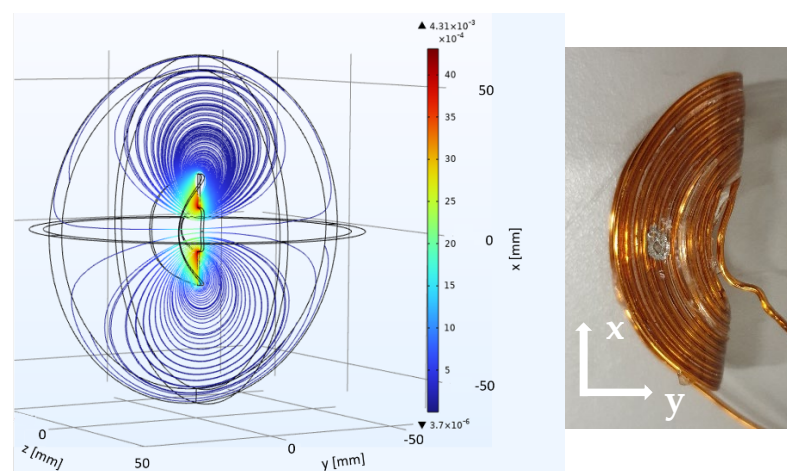


Figure 2. (Left): Simulation of the absolute value of the RF-field $|B_1(\mathbf{r})|$ of the homogenized version of the spirally wound, bent surface coil. The coils’ geometry is indicated by the inner black lines, while $|B_1(\mathbf{r})|$ is color encoded along the scale from blue (low values) to red (high values) and shown along

the three spatial coordinates. **(Right):** A picture of the coil with the coordinate system. The sample is aligned along x and positioned centric to the coil.

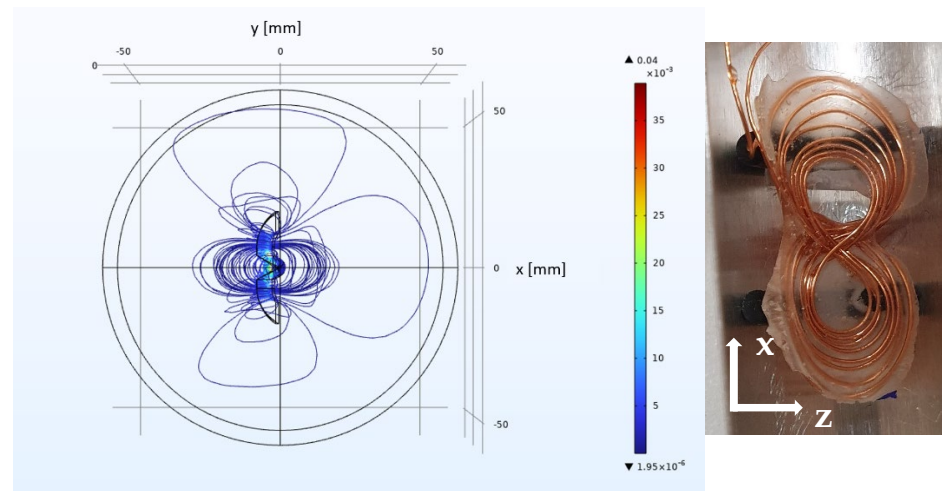


Figure 3. **(Left):** Simulation of $|B_1(r)|$ of the homogenized bent figure-8 coil. The coils geometry is indicated by the inner black lines, while $|B_1(r)|$ again is color encoded. The field plot shows two condensation areas at both openings of the coil. **(Right):** A picture of the figure-8 coil with the coordinates x and z . The sample is positioned along z , centric to the middle of the coil. The long axis of the cylindrical samples or tubes is aligned along x .

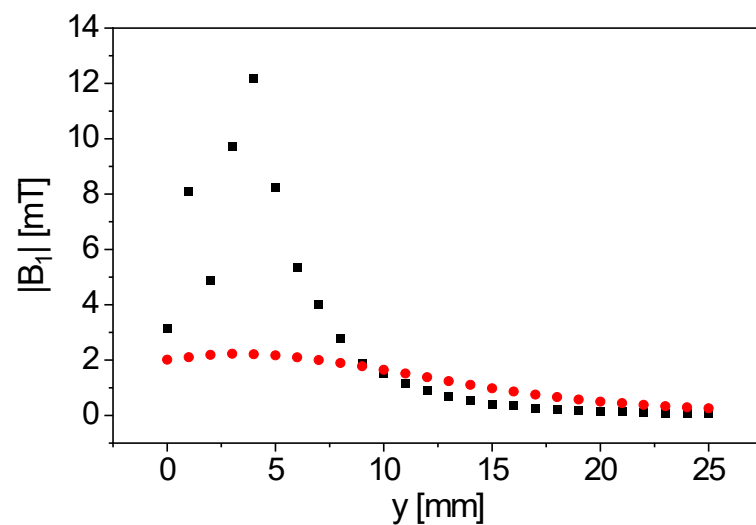


Figure 4. Simulated $|B_1|$ along y for the two coil geometries (■: figure-8 coil, ●: spirally wound, bent surface coil). $|B_1|$ of the figure-8 coil is larger than for the spirally wound, bent surface coil up to a distance of 9 mm, leading to an improved NMR sensitivity.




3.1.3. From Volume Coil to Surface Coil: Technical Realization of the Bent Surface Coils

During the manufacturing of a bent surface coil, the wire cannot be wound around a cylindrical carrier similar to how it is performed for solenoidal volume coils. Thus, the insulated copper wire was positioned on an adhesive film, and the wire was wound turn-by-turn as a flat geometry. Two-component, thermo-reversible epoxy glue, which does not lead to a significant background signal, was applied to permanently connect the windings. The glued coil was then bent to the desired shape after heat-softening the epoxy film. After cooling, the bent coil retains its geometry permanently which is then adapted to the cylindrical shape of a 10 mm tube containing a material stream. The motivation for bending was the expected larger filling factor and a more homogeneous B_1 field.

3.1.4. Comparison of the Coils: Technical Parameters and NMR Properties

Technical and NMR parameters are summarized for three different types of rf coils (Table 1). The solenoidal volume coil was previously used [12]. A spirally wound, bent surface coil is thus compared to the solenoidal volume coil and the bent figure-8 surface coil.

Table 1. Comparison of the technical and NMR parameters for the three types of rf coils.

Parameter	Solenoidal Volume Coil	Spirally Wound, Bent Surface Coil	Bent Figure-8 Surface Coil
Diameter/Size along x	13 mm	39 mm	24 mm
Number of turns	19	11	8
Diameter of the insulated copper wire	0.45 mm	0.8 mm	0.45 mm
Quality factor of rf circuit	318	168	147
90° pulse duration (16 dB attenuation)	13 μ s	30 μ s	9 μ s
Receiver dead time (RDT)	25 μ s	10.9 μ s	11 μ s
Typical receiver gain for a 10 mm water sample	68 dB	86 dB	70 dB
Profile width along x (left and right points at 10% from maximum)	4.3 mm; 21.2 mm	3.8 mm; 23.8 mm	0.4 mm; 19.6 mm
Distance at half signal along y	n.a.	2.5 mm	3.5 mm
Picture of the coil			

The NMR characteristics (Table 1: pulse duration, receiver gain, profile, etc.) were measured via the Hahn-echo sequence at a small echo time without an increment of τ_e [33]. Thus, the signal intensity was measured step-by-step to determine the profile along x and y . Care was taken to use samples with sufficiently small dimensions along the coordinates, along which the profiles were investigated. The different coil geometries influence parameters such as the flip angle, the receiver dead time (RDT), or the necessary receiver gain. RDT plays a significant role in selecting the planned application area of the sensor. Graphite slurries already exhibit short transverse relaxation times.

An important characteristic of an NMR probe is its sensitive volume. The normalized intensity $I/I_{\max, x}$ is therefore compared for the three types of coils. The Hahn-echo sequence was used at $\nu_L = 22.18$ MHz to determine the signal intensity as a function of x (Figure 5). $I_{\max, x}$ is the maximal signal intensity over x observed for each specific coil.

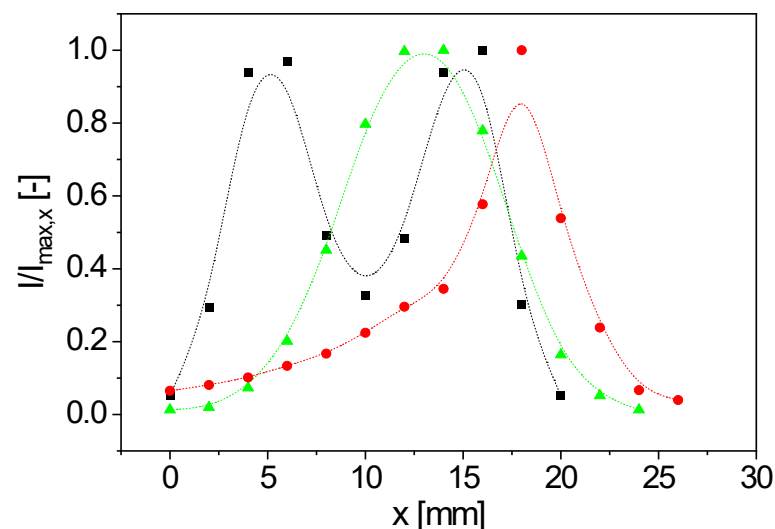


Figure 5. Measured normalized signal intensity profiles along x with a small water sample for the three different coil geometries (■: figure-8 coil, $\nu_L = 22.18$ MHz; ●: spirally wound, bent surface coil, $\nu_L = 21.99$ MHz; ▲: solenoidal coil, $\nu_L = 22.0$ MHz). The sample was moved in 2 mm incremental steps

along x (coordinate system of Figure 1). Pulse duration and frequency were kept constant for each coil. The geometries exhibit different intensity profiles along x . The solenoidal coils and the spirally wound, bent surface coils show a single intensity maximum, while two maxima were measured for the bent figure-8 coil, with approximately the same normalized signal intensity.

These x -intensity profiles (Figure 5) were measured with a 5 mm NMR tube (filling level 2 mm) with globally determined pulse durations. The sample, with its small filling level, was stepped through the magnet along x while the NMR signal intensity of a Hahn echo was measured at the indicated positions. Concerning the y and z positions: the sample was positioned directly on the surface of the surface coils without touching them and in the center of the volume coil, respectively. Two regions of maximal signal intensity were found near the two openings of the figure-8 coil (Figure 5). B_0 of the permanent magnet depends on x , due to the design of the V-shaped magnet, as does $v_L(r)$, consequently. In the realized optimal coil position, the same Larmor frequency is observed at the lower and the upper half of the figure-8 coil, which is reflected in the almost identical signal intensities at $x = 6$ mm, and $x = 16$ mm (Figure 5) at $v_L = 22.18$ MHz. The two maxima in Figure 5, however, are unique for the figure-8 coil, and correspond to the two maxima in $|B_1(r)|$, as evident from the simulation (Figure 3).

The y -profile of signal intensity was measured with rubber on a 10 mm NMR tube. On its outside, a rubber sheet (thickness 1 mm) was glued to provide a relatively thin sample for measuring the distance profile (Figure 6). $y = 0$ mm is therefore defined directly on the surface of the coils. The measurements show that the maximal signal intensity is not directly at the surface of the bent figure-8 coil, but at a distance of 2 mm, in agreement with the B_1 simulation (Figure 4). The sample was detectable up to a distance of $y = 7$ mm. This implies that not the entire volume of a sample with a diameter of 10 mm is detected. The position of the maximal signal intensity at a distance of 2 mm from the coil surface means that the most sensitive area of the inline-capable probe is in the sample itself when using tubes with a wall thickness smaller than 2 mm. For comparison, the realized sample tube for inline measurements has a wall thickness of 1 mm.

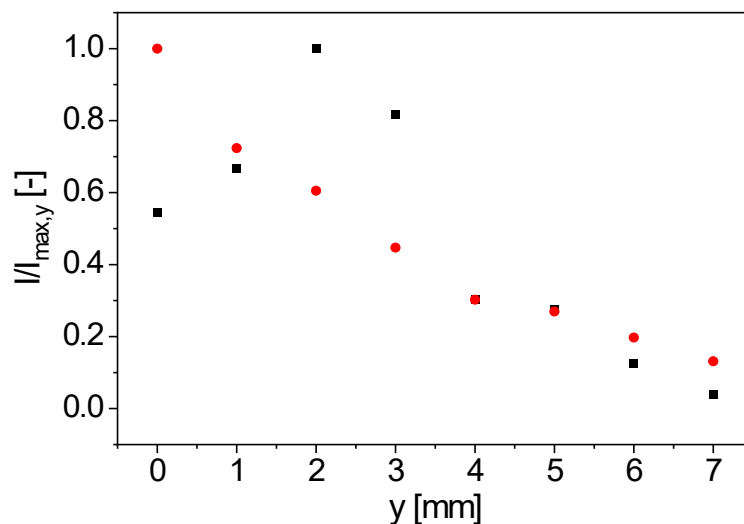


Figure 6. y -profiles of the normalized signal intensity for the bent figure-8 coil (■) and the spirally wound, bent surface coil (●), measured with a thin rubber sample. The maximal signal intensity for the spirally wound, bent surface coil is near the surface of the coil, whereas the maximum for the bent figure-8 coil is shifted by around 2 mm in the y -direction.

3.2. NMR-Measurements on Disperse Suspensions

An aqueous, extruded anode slurry was analyzed with a solid content of 50% w/w for the anode manufacturing of lithium-ion batteries (48.5% w/w graphite, 1% w/w CMC, 0.5% w/w carbon black). The sample temperature was 25 °C, and the long axis of the 10 mm

sample tube parallel to x was along the gravity direction. The filling level was 10 cm to guarantee a good sample homogeneity in the sensitive volume. The results were obtained with the figure-8 coil. The CPMG pulse sequence (Carr-Purcell-Meiboom-Gill) [34,35] was used with 3000 echoes, while τ_e was incremented. The repetition time was 2 s. It is well known that the transverse magnetization decay depends on the magnetic field gradient, leading to a sensitivity towards diffusion phenomena [34,35]. Please note that the magnetic field B_0 of the V-shaped sensor shows magnetic field gradients in all spatial dimensions, similar to the facts in other dedicated NMR sensors [32,36,37]. Therefore, only the average magnetic field gradient contributes in the measurements, which depends on the sample volume and the position of the RF coil. The signal decays were modeled by a mono-exponential function with sufficient numerical accuracy, leading to the effective transverse relaxation rate $R_{2,\text{eff}}$. $R_{2,\text{eff}}$ depends on τ_e (Figure 7, [23]), as expected. However, an effective diffusion coefficient in the slurry cannot be calculated via linear regression. The echo times τ_e are relatively small, so that, among other factors, sample heating and consequently, convection occur. Both relaxation and diffusion depend on the sample temperature. The RF energy intake leads to an increase of the temperature for small τ_e , in particular. The graphite particles in the slurry may additionally act as energy absorbers. In principle and in summarizing, measurements at a larger τ_e would be required. Additional measurements were performed with a reference sample to prove this data interpretation hypothesis.

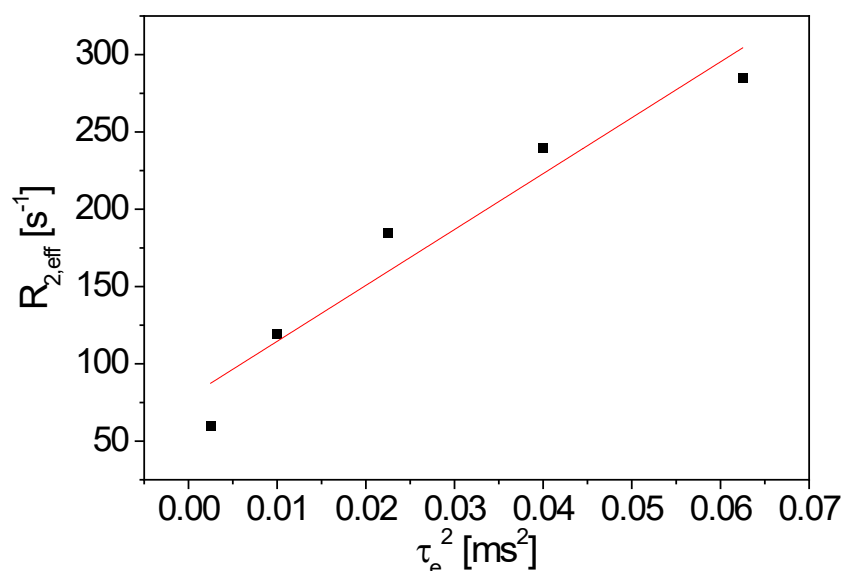


Figure 7. $R_{2,\text{eff}}$ as a function of the squared echo time τ_e^2 for an anode slurry of 48.5%w/w graphite, 1%w/w CMC and 0.5%w/w carbon black. The red line evidently shows the deviation from pure transverse relaxation and diffusion contributions.

The reference sample (20% H_2O , 80% D_2O and 0.1% CuSO_4) was filled into a completely filled 5 mm NMR tube. The average static gradient was determined via the Hahn echo sequence (increment factor for τ_e : 1.3; recycle delay: 10 s) to $G = 1.05 \text{ T/m}$ with $D = 2.4 \cdot 10^{-9} \text{ m}^2/\text{s}$ at $27 \text{ }^\circ\text{C}$ and $R_2 = 2 \text{ s}^{-1}$ (Figure 8 left). Deviations between the measured points and the modeling are due to experimental noise (magnitude data) and the inherent distribution of G .

In a first CPMG measurement on the reference sample, τ_e was varied in the range [0.05, 1.8] ms with a recycle delay of 4 s (Figure 8, right, black dots). A deviation from the expected linear relation $R_{2,\text{eff}}(\tau_e^2)$ was observed for a small τ_e , which was also in this case of measurements on the reference sample. To further test the hypothesis of sample heating and associated convection, the experiment was repeated. The repetition time was extended to 40 s to ensure thermostating of the sample. The sample filling height was reduced to 1 cm, and τ_e was reduced, in addition to comparing to the first measurement (Figure 8, right, red dots). As a result, the linear range is extended over a significantly larger range of τ_e ,

and the calculation of the diffusion coefficient with $G = 1.14 \text{ T/m}$ results in $D = 2.9 \cdot 10^{-9} \text{ m}^2/\text{s}$, which is within the expectation, considering the distribution of G and the sample heating.

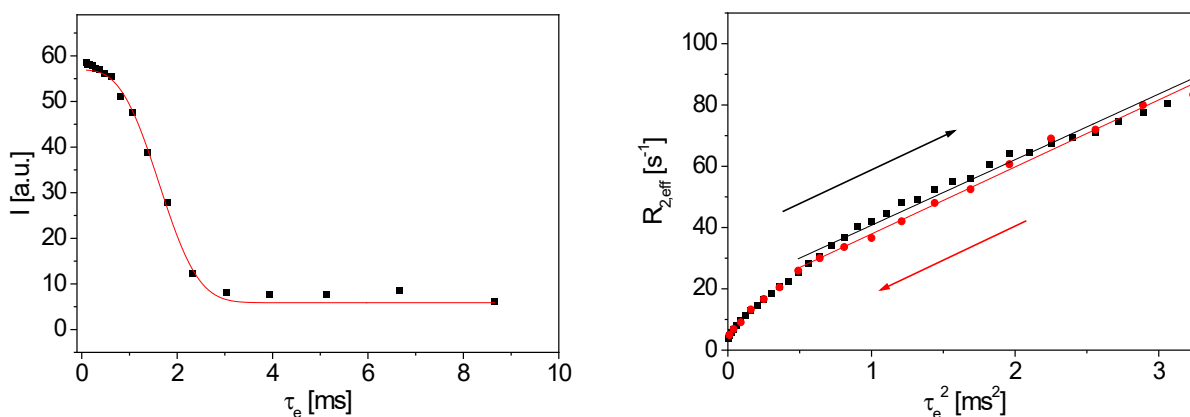


Figure 8. (Left): Measurements on the reference sample. Hahn-echo decay was used to determine the static gradient near the maximum sensitivity of the bent figure-8 coil ($G = 1.14 \text{ T/m}$). Modelling of the magnetization decays includes an offset. (Right): A deviation from the expected linear behavior of $R_{2,\text{eff}}(\tau_e^2)$ is found for a small τ_e due to sample heating. At large τ_e and a reduced sample filling level (red dots), RF heating is less significant, and the range of linearity is larger.

Please note that the significant difference in $R_{2,\text{eff}}$ of the two samples, the reference sample (Figure 8) and the graphite slurry (Figure 7). In contrast to the reference sample, τ_e was one order of magnitude smaller ($\tau_e \in [0.05, 0.25] \text{ ms}$) in the case of the graphite slurry, since $R_{2,\text{eff}}$ is much larger.

Diffusion is expected to be hindered in the slurry, leading to a reduction, i.e., a flatter dependence on τ_e , while R_2 is enhanced by paramagnetic relaxation enhancement due to nanoscale Fe and Fe oxides in typical concentrations up to 50 ppm in the used graphite powder.

Coming back to the potential application of the inline capable V-sensor, an important question concerns sedimentation which would influence the subsequent processing steps of coating, calendaring, and drying. The V-shaped sensor equipped with the figure-8 surface coil can be easily used to investigate the status of a slurry in a pipe. Positioning the magnet such that the gravity axis is along y (Figure 1) allows the investigation of the pipe's interior, which is, with its long axis, also perpendicular to the gravity axis, i.e., along y . The sensor can be placed exemplarily on top or on bottom of the pipe (Figure 9). In the case that significant sedimentation occurred in the optically opaque slurry, the effective transverse relaxation will tend toward the values of water, while the bottom part will show faster effective transverse relaxation due to, among other effects, paramagnetic relaxation enhancement.



Figure 9. Positioning of the surface coil on the bottom (left) and the top (right) of the horizontally fixed 10 mm pipe.

Thus, the anode slurry in a 10 mm pipe was fixed horizontally for 20 h to show whether sedimentation already occurs in the graphite slurry on that relatively short time scale. To investigate long-term effects, the sample was stored at the same position for seven days for a second measurement. CPMG measurements were carried out on the sedimented sample

with the figure-8 coil at the bottom and on top of the sample tube, to analyze the specific areas inside the tube (Figure 9). $R_{2,\text{eff}}$ for the two positions was measured for six values of τ_e (Figure 10).

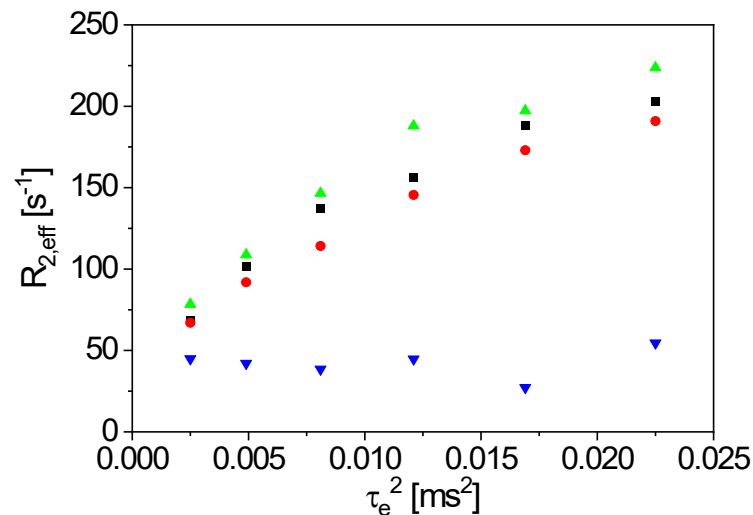


Figure 10. $R_{2,\text{eff}}(\tau_e^2)$ for an anode slurry of 48.5%w/w graphite, 1%w/w CMC and 0.5%w/w carbon black, measured with the bent figure-8 coil on top and on the bottom of the horizontally fixed sample tube (■: bottom, 20 h; ●: top, 20 h; ▲: bottom, 7 days; ▼: top, 7 days). $R_{2,\text{eff}}$ is larger at the bottom than at the top of the tube for both waiting times. $R_{2,\text{eff}}$ is clearly larger at the bottom of the sample with a 7 day waiting time (▲), while value at the top (▼) approaches the values for doped water.

The findings are in agreement with the observations described above: $R_{2,\text{eff}}$ increases with τ_e for the top and the bottom position in the first measurement (20 h). $R_{2,\text{eff}}$ is smaller for all τ_e at the top of the tube compared to the values at the bottom. This indicates the beginning of sedimentation due to the relaxation rates of “pure” water and water in the graphite sediment, containing paramagnetic impurities. Again, the measured points deviate slightly from a straight line, indicating sample heating. After a waiting time of seven days, the difference in relaxation between the position is even more evident: $R_{2,\text{eff}}$ at the bottom position only slightly increased compared to the first measurement. $R_{2,\text{eff}}$ lowered significantly at the top and is about constant with the small measured range of τ_e . Sedimentation in the graphite slurry causes $R_{2,\text{eff}}$ to approximate values at the top, similar to those measured on doped water. Please note again the small values of τ_e , as significantly larger echo times would have to be measured to determine the diffusion coefficient from the slope. The lower $R_{2,\text{eff}}$ results from a lower local concentration of graphite particles because of the longer sedimentation time. Nevertheless, the value of $R_{2,\text{eff}}$ is larger than that for pure water due to dissolved ions from the graphite particles. The results indicate that sedimentation is an issue even in the slurries of technically relevant composition.

4. Conclusions

The inline-capable NMR sensor with its dedicated hardware configuration was characterized. Different coil geometries were compared with the finding that the bent figure-8 coil is the shape with optimal characteristics for the desired application from the perspective of quality control. Simulations were carried out and compared to the measurement results. The V-shaped NMR sensor, equipped with the bent figure-8 surface coil, has the potential to be used in quality control, for example in battery anode production, based on the relaxation and diffusion properties of the used materials. The application is not limited to graphite slurries but can be extended to other mixtures and disperse systems and enables both offline and mobile inline NMR measurements.

Author Contributions: Conceptualization, E.S. and G.G.; methodology, E.S., T.R. and G.G.; validation, E.S., T.R. and G.G.; formal analysis, E.S., T.R. and G.G.; investigation, E.S., S.R. and T.R.; resources, H.N. and G.G.; data curation, E.S. and T.R.; writing—original draft preparation, E.S., T.R. and G.G.; writing—review and editing, E.S., S.R., T.R., H.N. and G.G.; supervision, G.G.; project administration, G.G.; funding acquisition, H.N. All authors have read and agreed to the published version of the manuscript.

Funding: This research was funded by the German Federal Ministry of Education and Research, grant number 03XP0359B. The responsibility for the content of this publication lies with the author.

Institutional Review Board Statement: Not applicable.

Informed Consent Statement: Not applicable.

Data Availability Statement: The data are available on request to the authors.

Acknowledgments: The authors thank financial support within the BMBF project Aqua-IQ-EL. The authors also sincerely thank the Bruker BioSpin GmbH, μ -imaging group, for their support during the development of the sensor. Stefanie Margiotta-Neu is kindly acknowledged for construction and technical drawings. We would like to thank the mechanical workshop at MVM-VM for the fabrication of all the parts of the probe. Juan Meza and Kevin Raczka are acknowledged for sample provision. The Deutsche Forschungsgemeinschaft is thanked for the substantial financial contribution in form of NMR instrumentation, Sachbeihilfe, within the instrumental facility Pro²NMR.

Conflicts of Interest: The authors declare no conflict of interest. The funders had no role in the design of the study; in the collection, analyses, or interpretation of data; in the writing of the manuscript; or in the decision to publish the results.

References

1. Rudszuck, T.; Förster, E.; Nirschl, H.; Guthausen, G. Low-field NMR for quality control on oils. *Magn. Reson. Chem.* **2019**, *57*, 777–793. [[CrossRef](#)] [[PubMed](#)]
2. Kern, S.; Wander, L.; Meyer, K.; Guhl, S.; Muckula, A.R.G.; Holtkamp, M.; Salge, M.; Fleischer, C.; Weber, N.; King, R.; et al. Flexible automation with compact NMR spectroscopy for continuous production of pharmaceuticals. *Anal. Bioanal. Chem.* **2019**, *411*, 3037–3046. [[CrossRef](#)] [[PubMed](#)]
3. van Beek, T.A. Low-field benchtop NMR spectroscopy: Status and prospects in natural product analysis. *Phytochem. Anal.* **2020**, *32*, 24–37. [[CrossRef](#)] [[PubMed](#)]
4. Dalitz, F.; Cudaj, M.; Maiwald, M.; Guthausen, G. Process and reaction monitoring by low-field NMR spectroscopy. *Prog. Nucl. Magn. Reson. Spectrosc.* **2012**, *60*, 52–70. [[CrossRef](#)] [[PubMed](#)]
5. Nordon, A.; McGill, C.A.; Littlejohn, D. Process NMR spectrometry. *Analyst* **2001**, *126*, 260–272. [[CrossRef](#)] [[PubMed](#)]
6. Perlo, J.; Demas, V.; Casanova, F.; Meriles, C.A.; Reimer, J.; Pines, A.; Blümich, B. High-resolution NMR spectroscopy with a portable single-sided sensor. *Science* **2005**, *308*, 1279. [[CrossRef](#)]
7. Raich, H.; Blümmler, P. Design and construction of a dipolar Halbach array with a homogeneous field from identical bar magnets: NMR Mandhalas. *Concepts Magn. Reson. Part B Magn. Reson. Eng.* **2004**, *23*, 16–25. [[CrossRef](#)]
8. Danieli, E.; Mauler, J.; Perlo, J.; Blümich, B.; Casanova, F. Mobile sensor for high resolution NMR spectroscopy and imaging. *J. Magn. Reson.* **2009**, *198*, 80–87. [[CrossRef](#)]
9. Litvinov, V.M.; Steeman, P.A.M. EPDM-carbon black interactions and the reinforcement mechanisms, as studied by low-resolution ¹H NMR. *Macromolecules* **1999**, *32*, 8476–8490. [[CrossRef](#)]
10. Blümich, B.; Blümmler, P. NMR Imaging of Polymer Materials. *Makromol. Chem. Macromol. Chem. Phys.* **1993**, *194*, 2133–2161. [[CrossRef](#)]
11. Windt, C.W.; Soltner, H.; van Dusschoten, D.; Blümmler, P. A portable Halbach magnet that can be opened and closed without force: The NMR-CUFF. *J. Magn. Reson.* **2011**, *208*, 27–33. [[CrossRef](#)] [[PubMed](#)]
12. Blümich, B.; Blümmler, P.; Eidmann, G.; Guthausen, A.; Haken, R.; Schmitz, U.; Saito, K.; Zimmer, G. The NMR-MOUSE: Construction, excitation, and applications. *Magn. Reson. Imaging* **1998**, *16*, 479–484. [[CrossRef](#)] [[PubMed](#)]
13. Veliyulin, E.; Mastikhin, I.V.; Marble, A.E.; Balcom, B.J. Rapid determination of the fat content in packaged dairy products by unilateral NMR. *J. Sci. Food Agric.* **2008**, *88*, 2563–2567. [[CrossRef](#)]
14. Guthausen, A.; Guthausen, G.; Kamlowski, A.; Todt, H.; Burk, W.; Schmalbein, D. Measurement of fat content of food with single-sided NMR. *J. Am. Oil Chem. Soc.* **2004**, *81*, 727–731. [[CrossRef](#)]
15. Rudszuck, T.; Zick, K.; Groß, D.; Nirschl, H.; Guthausen, G. Dedicated NMR sensor to analyze relaxation and diffusion in liquids and its application to characterize lubricants. *Magn. Reson. Chem.* **2021**, *59*, 825–834. [[CrossRef](#)] [[PubMed](#)]
16. Morin, D.M.; Yan, P.; Augustine, M.P.; Balcom, B.J. An Optimized 2 MHz Unilateral Magnet with a Large Homogeneous Sensitive Spot. *Appl. Magn. Reson.* **2022**, *53*, 401–415. [[CrossRef](#)]

17. Mandal, S.; Borneman, T.W.; Koroleva, V.D.; Hürlimann, M.D. Direct optimization of signal-to-noise ratio of CPMG-like sequences in inhomogeneous fields. *J. Magn. Reson.* **2014**, *247*, 54–66. [[CrossRef](#)]
18. Hürlimann, M.D. Encoding of diffusion and T1 in the CPMG echo shape: Single-shot D and T1 measurements in grossly inhomogeneous fields. *J. Magn. Reson.* **2007**, *184*, 114–129. [[CrossRef](#)]
19. Hürlimann, M.D. Carr-Purcell sequences with composite pulses. *J. Magn. Reson.* **2001**, *152*, 109–123. [[CrossRef](#)]
20. Hürlimann, M.D. Diffusion and Relaxation Effects in General Stray Field NMR Experiments. *J. Magn. Reson.* **2001**, *148*, 367–378. [[CrossRef](#)]
21. Hürlimann, M.; Griffin, D. Spin dynamics of Carr–Purcell–Meiboom–Gill-like sequences in grossly inhomogeneous B₀ and B₁ fields and application to NMR well logging. *J. Magn. Reson.* **2000**, *143*, 120–135. [[CrossRef](#)]
22. Hürlimann, M.D.; Helmer, K.G.; Deswiet, T.M.; Sen, P.N. Spin Echoes in a Constant Gradient and in the Presence of Simple Restriction. *J. Magn. Reson. A* **1995**, *113*, 260–264. [[CrossRef](#)]
23. Guthausen, A.; Zimmer, G.; Blümmler, P.; Blümich, B. Analysis of polymer materials by surface NMR via the MOUSE. *J. Magn. Reson.* **1998**, *130*, 1–7. [[CrossRef](#)]
24. Song, Y.-Q.; Venkataramanan, L.; Hürlimann, M.D.; Flaum, M.; Frulla, P.; Straley, C. T1-T2 correlation spectra obtained using a fast two-dimensional Laplace inversion. *J. Magn. Reson.* **2002**, *154*, 261–268. [[CrossRef](#)] [[PubMed](#)]
25. Hürlimann, M.D.; Venkataramanan, L. Quantitative measurement of two-dimensional distribution functions of diffusion and relaxation in grossly inhomogeneous fields. *J. Magn. Reson.* **2002**, *157*, 31–42. [[CrossRef](#)]
26. Kimmich, R. *NMR—Tomography Diffusometry Relaxometry*; Springer: Berlin, Germany, 1997.
27. Fukushima, E.; Roeder, S.B.W. *Experimental Pulse NMR, a Nuts and Bolts Approach*; Addison-Wesley Publishing Company Inc.: London, UK, 1981.
28. Lee, J.H.; Labadie, C.; Springer, C.S.; Harbison, G.S. 2-Dimensional Inverse Laplace Transform Nmr—Altered Relaxation-Times Allow Detection of Exchange–Correlation. *J. Am. Chem. Soc.* **1993**, *115*, 7761–7764. [[CrossRef](#)]
29. Grebenkov, D.S. Laplacian Eigenfunctions in NMR. II. Theoretical Advances. *Concepts Magn. Reson. Part A* **2009**, *34A*, 264–296. [[CrossRef](#)]
30. Ukkelberg, A.; Sorland, G.H.; Hansen, E.W.; Wideroe, H.C. ANAHESSE, A new second order Sum of Exponentials Fit Algorithm, Compared to the Tikhonov Regularization Approach, with NMR Applications. *IJRRAS* **2010**, *2*, 195–210.
31. Förster, E.; Nirschl, H.; Guthausen, G. NMR Diffusion and Relaxation for Monitoring of Degradation in Motor Oils. *Appl. Magn. Reson.* **2017**, *48*, 51–65. [[CrossRef](#)]
32. McDonald, P.; Aptaker, P.; Mitchell, J.; Mulheron, M. A unilateral NMR magnet for sub-structure analysis in the built environment: The Surface GARField. *J. Magn. Reson.* **2007**, *185*, 1–11. [[CrossRef](#)]
33. Hahn, E.L. Spin Echoes. *Phys. Rev.* **1950**, *80*, 580–594. [[CrossRef](#)]
34. Carr, H.Y.; Purcell, E.M. Effects of Diffusion on Free Precession in Nuclear Magnetic Resonance Experiments. *Phys. Rev.* **1954**, *94*, 630–638. [[CrossRef](#)]
35. Meiboom, S.; Gill, D. Modified spin-echo method for measuring nuclear relaxation times. *Rev. Sci. Instrum.* **1958**, *29*, 688–691. [[CrossRef](#)]
36. Eidmann, G.; Savelsberg, R.; Blümmler, P.; Blümich, B. The NMR MOUSE, a mobile universal surface explorer. *J. Magn. Reson. A* **1996**, *122*, 104–109. [[CrossRef](#)]
37. Zimmer, G.; Guthausen, A.; Blümich, B. Characterization of cross-link density in technical elastomers by the NMR-MOUSE. *Solid State Nucl. Magn. Reson.* **1998**, *12*, 183–190. [[CrossRef](#)] [[PubMed](#)]

Disclaimer/Publisher’s Note: The statements, opinions and data contained in all publications are solely those of the individual author(s) and contributor(s) and not of MDPI and/or the editor(s). MDPI and/or the editor(s) disclaim responsibility for any injury to people or property resulting from any ideas, methods, instructions or products referred to in the content.